Orthorhombic-tetragonal transition in twin-free (110) $YBa_2Cu_3O_7$ films

F. Miletto Granozio*
Istituto Nazionale di Fisica della Materia (I.N.F.M.), Sezione di Napoli, Napoli, Italy and CEA Grenoble, DRFMC\SPSMS\LCP, 17 rue de Martyrs, 38054, Grenoble, Cedex 9, France

F. Ricci
Dipartimento Scienze Fisiche dell'Università di Napoli Federico II, Napoli, Italy

U. Scotti di Uccio
Istituto Nazionale di Fisica della Materia (I.N.F.M.), Sezione di Napoli, Napoli, Italy and Dipartimento Scienze Fisiche dell'Università di Napoli, Federico II, Napoli, Italy

J. C. Villegier
CEA Grenoble, DRFMC\SPSMS\LCP, 17 rue de Martyrs, 38054, Grenoble, Cedex 9, France
(Received 18 August 1997)

Twin-free (110) $YBa_2Cu_3O_7$ films have been grown by pulsed laser deposition on vicinal (110) STO substrates making use of a double $PrBa_2Cu_3O_7$ template layer. Such samples offer a unique opportunity to analyze the physics of the tetragonal-orthorhombic transition and of strain relaxation, and to investigate the fine details of the film-substrate alignment. Mapping of relevant regions of reciprocal space has been performed by x-ray diffraction, and a clear interpretation of the complex experimental data has been obtained after attentive analysis. The presence of a strained layer characterized by an angle $\gamma > 90°$ between the *a* and *b* axes has been observed. The details of the tetragonal-orthorhombic transition have been investigated by repeating reciprocal-space mapping (*a*) after oxygen depletion of a measured sample, and (*b*) after restoring the former oxygen content. The mechanisms of detwinning, strain relaxation, and epitaxial alignment taking place during the tetragonal-orthorhombic transition are discussed in detail. [S0163-1829(98)03606-6]

I. INTRODUCTION

YBCO thin films with excellent superconducting properties are commonly obtained by deposition onto perovskites, such as $SrTiO_3$ (STO), $LaAlO_3$ (LAO), $NdGaO_3$ (NGO), etc. Such substrates are very stable at typical YBCO deposition conditions, so that the possibility of chemical reactions or interdiffusion is inhibited. Moreover, the similarity of the crystal structure and the low lattice mismatch allow epitaxial growth. Growth orientation has been shown to depend drastically on deposition conditions, and *c* axis in-plane orientations are only obtained at low deposition temperatures. A crossover from (100) to (001) growth has been demonstrated when YBCO is grown onto (100) STO, (100) LAO, or (110) NGO;[1,2] a similar crossover between (110) and (103)/(013) orientations (see Fig. 1) is found instead on (110) STO (Refs. 3 and 4) and (100) NGO.[4]

The ability of growing YBCO films with different orientations allows one to take advantage of the anisotropy of this material. Even though less studied with respect to the most commonly employed (001) oriented films, (110) YBCO films are very interesting for several reasons. The highly conductive Cu-O planes are perpendicular to the substrate. Moreover, all the grains have the *c* axis aligned in the same direction, that is, along the in-plane [001] axis of the substrate. This is not the case for (100) films, unless special substrates are employed.[5] Therefore, (110) films show very anisotropic transport properties, both in the normal and in the superconductive state.[2,4] The coherence length is also anisotropic, with a relatively large value in the (001) plane, that is, also in the direction perpendicular to the substrate surface. These peculiarities make these films promising candidates for application in various configurations of tunnel and Josephson junctions, and in superconducting three-terminal devices.

In a number of papers,[3,6–9] procedures are described to prepare single phase (110) films with high critical temperatures. In most cases, the substrate is (110) STO, because of

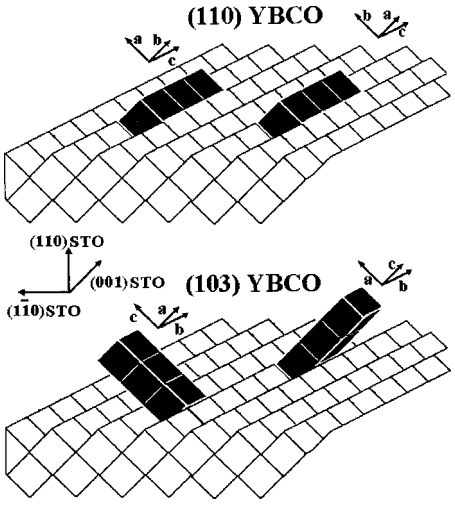

FIG. 1. Sketch of the possible epitaxial relations between the YBCO cell and a (110) STO substrate.

the good fit between its lattice parameter ($a_{STO} \approx 3.90$ Å) and those of YBCO. A procedure for the deposition of pure (110) oriented YBCO films possessing critical temperatures close to the bulk values, based on a single deposition temperature has been reported in Ref. 4. Nevertheless, single deposition temperature procedures have been usually found to fail, since the competing growth of (103) and (013) orientations[10] takes place at optimal YBCO deposition temperature. The required deposition temperature for (110) YBCO growth is, in fact, so low that many defects are incorporated in the film due to reduced cation mobility, resulting in poor structural and superconductive properties. One way to circumvent this problem is to resort to the template or self-template technique, first introduced to prepare (100) YBCO films.[11,12] A buffer layer of YBCO (Refs. 8 and 9) or PBCO (Refs. 3, 7, and 8) is deposited at low substrate temperature T_s, leading to (110) growth. As a second step, the temperature is raised up to the optimal value for YBCO deposition.

As for other orientations, it is expected that many properties of (110) YBCO films are tightly connected to the fine details of the crystal structure. This, in turn, is determined by the crystal structure of the terminating atomic plane of the substrate, and by its defects, as well as by deposition conditions. X-ray diffraction (XRD) (Refs. 3, 4, and 6) and transmission electron microscopy (Refs. 8 and 13) investigations have thrown some light on the microstructure of (110) films and on their habits of growth. However, there are interesting features regarding the transition of (110) YBCO from the tetragonal (T) to orthorhombic (O) phase and the effects of strain that have not yet been investigated, and that stimulated the present work. Such features are briefly reported in the following:

(i) During the T-O transition, the projection of the YBCO unit cell on the (001) plane is transformed in a rectangle possessing two sides that differ by about 1.5%. In the case of (001) YBCO growing on (100) $SrTiO_3$ substrates, it has been reported that the YBCO cell undergoes a rotation of about 0.5° around the (001) direction in order to keep its [110] direction aligned with the [110] or [1$\bar{1}$0] direction of the substrate.[14] In the case of (110) films, no report about the details of axes alignment is available to our knowledge.

(ii) In c-axis films, the T-O transition is characterized by the formation of a-b twin domains. The a-b twinning allows the film to relax part of the strain at the interface with the substrate. In fact, the twinning restores the tetragonal symmetry at the macroscopic level.[15] One route to the suppression of twinning is to resort to noncubic substrates such as NGO,[16] showing a nearly perfect match of lattice parameters with those of the film. In the case of (110) YBCO films, the lengths of the axes which lie parallel to the substrate surface (i.e., [001] and [110]), are instead not affected by the exchange between a and b. Therefore, the twinning cannot lead to elastic energy reduction. On the contrary, twinning adds a positive surface energy contribution due to the interfaces between different domains. Therefore, the formation of twinned domains has to be attributed to the presence of thermal fluctuations during a ferroelastic transition, as in the case of single crystals,[17] and not also to strain energy reduction, as in the case of c-axis films. The former considerations suggest that even a small perturbation of the symmetry of the in-plane substrate lattice, as the one induced by a vicinal cut, could induce the formation of single domain (110) films.

(iii) In order to match the STO lattice, a relatively large strain of the (110) YBCO film is required. Due to the anisotropy of the YBCO structure, it is not easy to determine *a priori* what the deformation of the structure will be.

In order to investigate the aforementioned items, pure (110) oriented YBCO films have been deposited by laser ablation on vicinal (110) STO substrates making use of a PBCO template layer. The use of YBCO as a self-template layer was avoided, since such a technique appears to be less reliable on the basis of current literature, and has been proved in some cases unsuccessful.[3] Substrates are characterized by a 0.5° tilt of substrate surface from (110) into (010); that is, the [001] axis is parallel to the substrate surface, while the [110] axis is tilted by 0.5° out of the substrate surface. Experimental investigations are principally based on reciprocal space mapping (RSM) performed by x-ray diffraction. Results of structural characterization of a sample after several thermal cycles are also reported.

II. EXPERIMENTAL

Fabrication of the PBCO/YBCO bilayers was carried out in a pulsed laser deposition system equipped with four targets and a load lock, allowing *in situ* growth of multilayer structures. All the steps of the fabrication process were controlled by a personal computer. Sintered PBCO and YBCO targets were ablated by the beam of an excimer laser ($\lambda = 248$ nm), with pulse duration $\tau = 30$ ns, repetition rate of 3 Hz and energy density of about 2 J cm^2. Deposition rate was ≈ 0.1 nm/sec and O_2 pressure during deposition was 25 Pa. After deposition, O_2 was injected in the deposition chamber at a pressure of 0.8×10^5 Pa, and a temperature of about 650 °C, the substrate was first cooled to 500 °C and then, after 20 min, to room temperature.

Before the YBCO/PBCO deposition, STO substrates were degreased and an amorphous YBCO film was deposited at ambient temperature on the back of the substrate in order to enhance coupling with the radiation of a resistive filament employed for the heating. Careful adjustments of the multilayer deposition process were required in order to optimize the superconducting properties of thin and ultrathin YBCO films while preserving pure (110) orientation. As a result, the following procedure was chosen:

(i) A first PBCO template layer with thickness of 30 nm was deposited on the (110) substrates at the temperature $T = 650$ °C in order to induce (110) orientation in the following layers.

(ii) A second PBCO layer with thickness 20 nm was deposited on the previous layer at higher temperature ($T = 750$ °C) in order to enhance the crystal quality of the surface where the YBCO film was deposited.

(iii) Finally, YBCO films of variable thickness where deposited on the double PBCO template layer.

A detailed report on the superconducting properties of the YBCO films on double template layer will be reported elsewhere. Briefly, T_c regularly exceeded 88 K for films thicker than 80 nm, while a relatively fast depression of T_c was

found down to thicknesses of 10 nm. In order to increase the diffracted intensity and decrease the acquisition time during reciprocal space mapping, only samples with thicknesses exceeding 300 nm were employed in the present work.

In order to study the effect of oxidation-deoxidation cycles on the structure of the samples, the following thermal treatments have been adopted: (a) 160 min annealing at 600 °C in vacuum. It is known that such a procedure fully removes oxygen from the chains of YBCO and PBCO, leading to tetragonal structure; (b) 45 min annealing at 450 °C and 2×10^4 Pa O_2 pressure. This process restores the former O_2 content in the film.

XRD analyses are performed on as-deposited films and after each thermal treatment. All the measurements reported in the following are relative to the same sample.

III. XRD CHARACTERIZATION

XRD analyses have been performed by using a standard two-axes diffractometer in Bragg-Brentano focusing geometry (Rigaku D/MAX-B). A third axis, allowing for the rotation of the samples around their surface normal (Φ scan), is also present. The Cu anode (Cu $K\alpha_1$:$\lambda=1.540598$ Å; Cu $K\alpha_2$:$\lambda=1.544418$ Å) is operated at 30 kV, 30 mA. The beam is collimated by Soller slits (4°) parallel to the scattering plane. A series of slits (divergence slit=0.15 mm; scattering slit=0.15 mm; receiving slit=0.05 mm) are employed in RSM measurements. The apparatus is equipped with a crystal graphite monochromator, curved in the scattering plane, that collimates the diffracted rays. Sample alignment is carefully controlled before each set of measurements. The alignment procedure also allows one to perform accurate measurements of vicinality, by determination of the angles between the substrate plane and the principal axes of STO. The experimental resolution achieved in rocking curves is better than 0.05° under typical experimental conditions.

RSM is a very powerful technique for studying orientation, strain, and twinning in epitaxial films, and has been already employed to investigate films deposited on (110) STO.[3,6] The relevant regions of reciprocal space have been firstly determined by calculation. Identification of Bragg and Laue zones and alignment of reciprocal spaces has been performed considering the case of a twinned YBCO film containing domains with (110) YBCO‖(110) STO and domains with (110)‖(110) STO. Mapping of the reciprocal space has been then performed in several distinct regions. The cross section of reciprocal space containing the [110] and [110] vectors of a (110) YBCO film is shown in Fig. 2. The zones around the (330) STO (region *A*), the (400) STO (region *B*), and the (040) STO (region *C*) reflections, where reciprocal space mapping was performed, are also indicated.

Mapping of region *C* is performed after a rotation around the normal to the substrate of an angle $\Phi=180°$, with respect to the position used for the mapping of region *B*. Therefore, the increasing ω (or $\Delta\omega$) directions in the maps of *B* and *C* correspond to opposite angular directions in the lattice. All the contour plots reported in the following are in log scale. The intensity ratio between two adjacent contour curves is about 3.

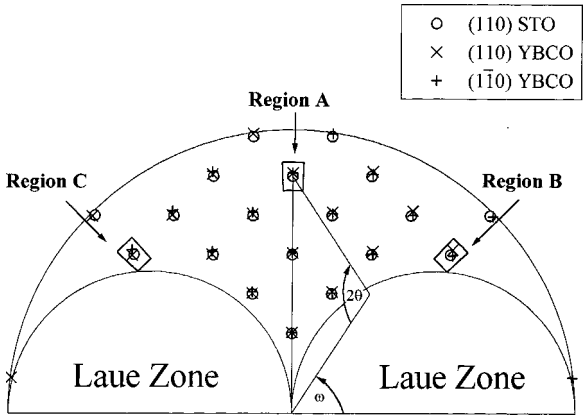

FIG. 2. Cross section of YBCO and STO reciprocal spaces, in between the [100] and [010] directions. Regions explored by reciprocal space mapping are marked. Note that the three (400) peaks [as well as the (040) peaks] are not aligned on an identical ω value.

A. Identification of growth orientation

Symmetric θ-2θ scans, routinely performed on (110) samples, do not show the presence of any spurious peak. In Fig. 3 the symmetric θ-2θ scan of a YBCO/PBCO bilayer is shown. The value of the (110) plane spacing ($d\approx0.2725$ nm) from the (330) reflection corresponds to unstrained YBCO. The presence of a strained fraction of the film with the same orientation will arise in the following, although its reflection in region *A* is covered by the substrate. We refer therefore to the unstrained fraction as relaxed YBCO/PBCO layer (*r*YP). As the relation $b\approx c/3$ holds for both YBCO and PBCO, and due to possible deviations from the bulk values of the lattice parameters, this analysis does not allow us to determine the possible content of (103)/(013) oriented grains. In fact, the peak attributed to YBCO may be (330) as well as (309), while (039) YBCO, if present, may partially overlap the (330) reflection of STO. Identification of such reflections as ''shoulders'' of (330) STO peak is questionable, also because of possible difference of the lattice parameters from bulk values. In order to rule out the presence of (103) or (013) growth, we resorted to reciprocal space mapping of samples. The absence of diffracted intensity in the region of the (00 11) YBCO reflection

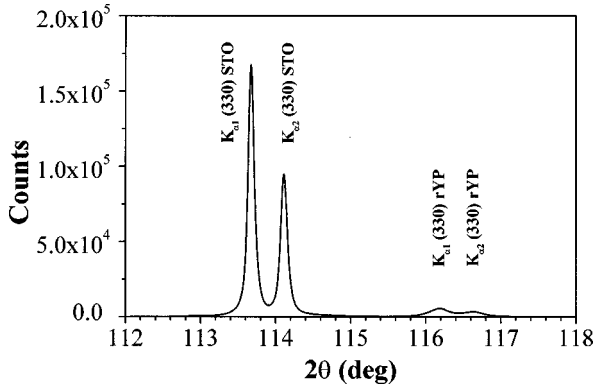

FIG. 3. θ-2θ symmetric scan over the (330) peaks of the STO substrate and of the YBCO/PBCO bilayer. The value of the lattice parameter ($d\approx0.2725$ nm) proves that the peak has to be attributed to an unstrained fraction of the YBCO/PBCO bilayer (*r*YP).

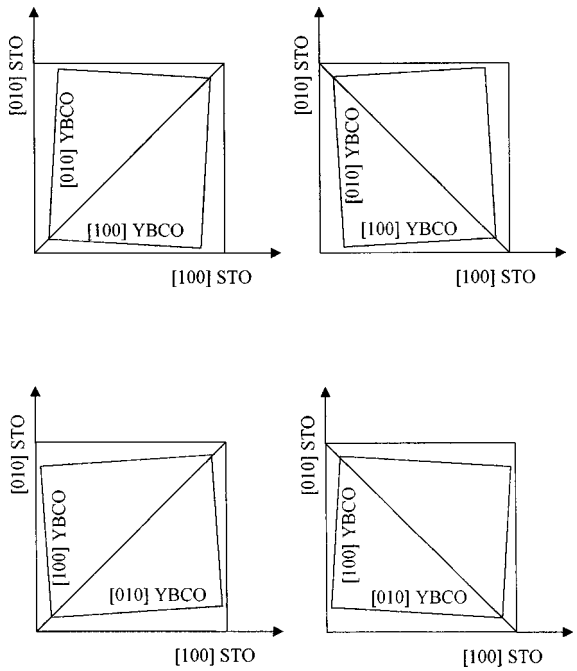

FIG. 4. Sketch of the possible epitaxial in-plane orientations of the *a*-*b* lattice of a (001) YBCO film on a (100) STO surface.

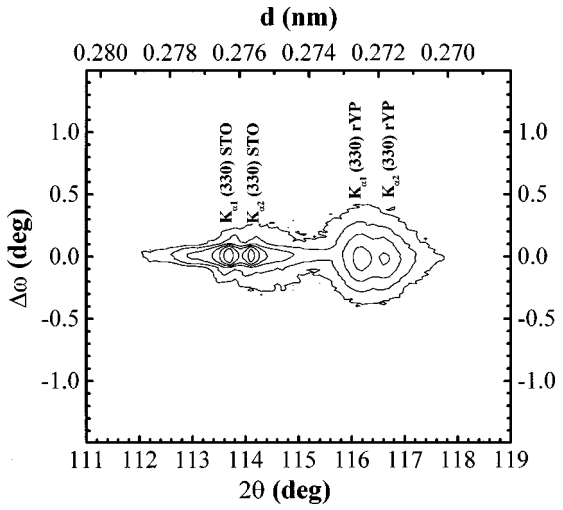

FIG. 5. Map of region *A* for a (110) YBCO/PBCO/STO bilayer deposited in standard conditions. The YBCO/PBCO peak is attributed, on the base of the lattice parameters values, to the relaxed portion of the bilayer. The peak corresponding to the strained portion is overlapped by the substrate reflection.

of (103) and (013) grains proves that pure (110) orientation is achieved within the experimental resolution ($\approx 1\%$).

B. Structure of the (110) YBCO/PBCO bilayer

Due to the *T*-*O* transition of YBCO and PBCO, the film structure undergoes a rearrangement during the cooling process. A sketch of the alignment of the in-plane axes of YBCO and STO in the case of *c*-axis films, is shown in Fig. 4. Four possible epitaxial relations are found,[14] due to the two different alignments of the diagonals ([110] YBCO∥[110] STO, or $[1\bar{1}0]$ YBCO∥$[1\bar{1}0]$ STO) and to twinning.

Effects of a similar rearrangement are also found in (110) growth. The mapping around the (330) STO reflection (region *A*) is shown in Fig. 5. In this plot, as in all the following ones, $\Delta\omega = \omega - \omega_{\mathrm{STO}}$, ω_{STO} being the position of the STO peak in the same region. $K_{\alpha 1}$ and $K_{\alpha 2}$ reflections of (330) YBCO/PBCO are clearly resolved. The full width at half maximum (FWHM) of the rocking curve of the $K_{\alpha 1}$ (330) YBCO is 0.18°. The map demonstrates that [110] YBCO∥[110] PBCO∥[110] STO, and excludes the presence of grains with [110] YBCO∥[110] PBCO∥[110] STO. In fact, the [110] direction of such grains should be tilted of an angle $\Delta\omega = \pm 1.0°$ off [110] STO or off [110] STO. This value is much larger than the observed rocking curve width of the (330) YBCO reflection.

Maps of a region around the nonsymmetric (400) STO and around the (040) STO reflections (regions *B*and *C*) are shown in Figs. 6(a) and 6(b), respectively. The map in Fig. 6(a) is characterized by the presence of three peaks from the YBCO/PBCO bilayer. The two principal peaks are both tilted by $\Delta\omega = -0.45°$ with respect to the (400) STO direction. The peak at 0.382 nm is unambiguously interpreted as the (400) reflection of unstrained YBCO (or YBCO/PBCO); such layer will be referred to in the following as relaxed YBCO/PBCO layer (*r*YP). The peak at $d = 0.387$ nm is interpreted as the (400) reflection of strained YBCO/PBCO (*s*YP), as discussed in the following. The weaker peak ($d = 0.393$ nm, $\Delta\omega = 0.29°$) is attributed to (040) *s*YP. The map in Fig. 6(b) also presents three peaks from the YBCO/PBCO bilayer. The strongest reflections are tilted by $\Delta\omega = 0.45°$ and $\Delta\omega = 0.29°$ with respect to (400) STO. The weaker one is tilted by $\Delta\omega = -0.45°$. Analogously with the case of Fig. 6(a), the three peaks are interpreted from the corresponding lattice parameters ($d = 0.393$, 0.389, and 0.387 nm) as (040) reflections of strained and unstrained YBCO/PBCO, and (400) reflections of strained YBCO/PBCO, respectively. Sharp rocking curves are obtained for all the reflections [FWHM = 0.23° for (400) and (040) *r*YP; FWHM = 0.22° for (400) and (040), *s*YP], proving the high quality of the crystal structure.

Data regarding the reflections found in regions *A*, *B*, and *C* of the as-deposited film are summarized in Table I.

C. Effect of thermal treatments

The sample deposited on vicinal STO, characterized by the measurements reported in Figs. 5 and 6, was annealed following the *a* procedure (see Sec. II). After this treatment, the sample became an electrical insulator. Mapping of the regions *A*, *B*, and *C* were successively performed. The map around the (330) STO symmetrical reflection is shown in Fig. 7. $K_{\alpha 1}$ and $K_{\alpha 2}$ (330) *r*YP peaks are detected, while the corresponding reflections of *s*YP, if any, would be overlapped by the more intense (330) STO peaks and cannot be separated. The sharpness of the rocking curve of the $K_{\alpha 1}$ (330) YBCO reflection (FWHM = 0.20°) proves that the quality of the crystal structure is not affected by this annealing process. Mapping of the nonsymmetrical reflections of region *B* and *C* are similar. In Fig. 8 data collected by analysis of region *B* are shown. Also in this case, reflections attributed to *r*YP are clearly shown [$K_{\alpha 1}$ and $K_{\alpha 2}$ (400) YBCO peaks], while the corresponding peaks of *s*YP would

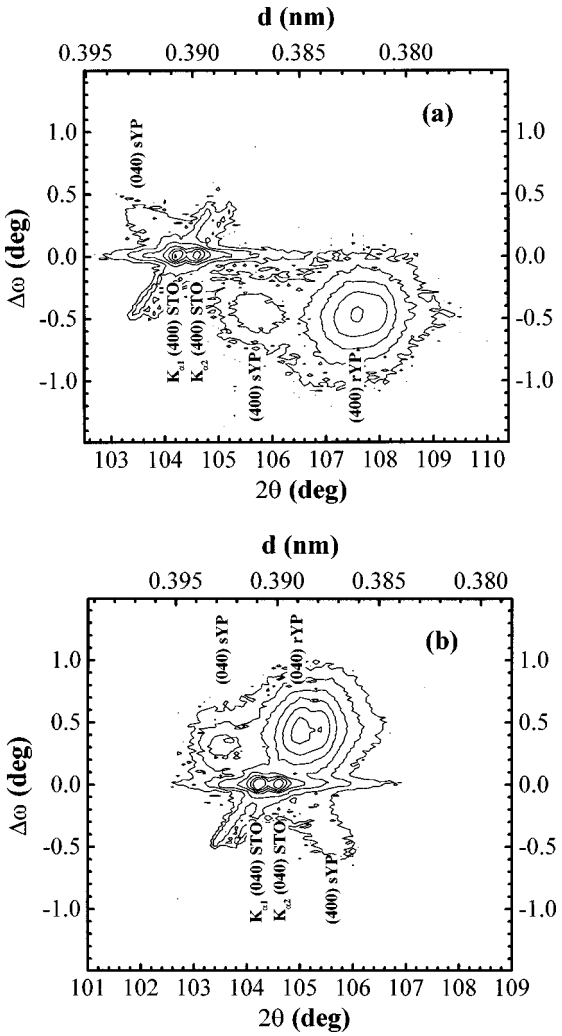

FIG. 6. Maps of regions *B* and *C*, as determined in Fig. 3, are shown in (a) and (b), respectively. The presence of three distinct peaks, belonging to the strained (*s*YP) and relaxed (*r*YP) portions of the bilayer clearly emerges.

be overlapped by substrate reflections. Data reported in Figs. 7 and 8 demonstrate that the YBCO/PBCO bilayer is in the tetragonal form. The following relations hold: [100] *r*YP∥[100] STO; [010] *r*YP∥[010] STO; [001] *r*YP∥[001] STO.

The second annealing, performed following the *b* procedure, restored the electrical conductivity of the sample. The structure was then investigated by mapping of the region *A* (Fig. 9), and of the regions *B* and *C* [Figs. 10(a) and 10(b)]. The measurements indicate that the YBCO/PBCO film is in the orthorhombic form. The values of the *a* and *b* lattice parameters are restored to the initial values within 1 pm. The thermal treatment is shown to affect some details in the orientation of (110) *r*YP. Traces of *s*YP are still found.

Interpretation of these maps is not as direct as in the case of as-deposited films, also because of a sensitive broadening of YBCO/PBCO rocking curves. The map of region *A* shows three different peaks that are attributed to (330) *r*YP, characterized by close values of lattice spacing, but different tilt angle. In the region *B*, the (400)*r*YP peak with maximum at $\Delta\omega\approx-0.4°$ is not symmetric, but it shows a tail extending

TABLE I. Summary of the data concerning maps of Figs. 5–10. The value indicated in the column $\Delta\omega$ is defined as the difference between the ω value of a peak and the ω value of the STO $K_{\alpha1}$ peak being in the same region.

	Figure	Reflection	*d* (nm)	$\Delta\omega$ (deg)
	5	(330) STO	0.276	0
	5	(330) *r*YP	0.272	0
	6(a)	(400) STO	0.390	0
	6(a)	(400) *r*YP	0.382	−0.45
As-deposited	6(a)	(400) *s*YP	0.387	−0.45
	6(a)	(040) *s*YP	0.393	0.29
	6(b)	(040) STO	0.390	0
	6(b)	(040) *r*YP	0.389	0.45
	6(b)	(040) *s*YP	0.393	0.29
	6(b)	(400) *s*YP	0.387	−0.45
	7	(330) STO	0.276	0
After thermal treatment	7	(330) *r*YP	0.273	0
(a)	8	(400) STO	0.390	0
	8	(400) *r*YP	0.386	0
	9	(330) STO	0.276	0
	9	(330) *r*YP	0.272	0, ±1
	10(a)	(400) STO	0.390	0
	10(a)	(400) *r*YP	0.382	−0.4÷0.4
After thermal treatment	10(a)	(040) *r*YP	0.389	−0.4
(b)	10(b)	(040) STO	0.390	0
	10(b)	(040) *r*YP	0.389	±0.4
	10(b)	(400) *r*YP	0.382	0.4
	10(b)	(040) *s*YP	0.393	0.3
	10(b)	(400) *s*YP	0.387	−0.4

up to $\Delta\omega\approx0.4°$. Furthermore, a broad (040) *r*YP peak is-also present, at an angle$\Delta\omega\approx-0.4°$. Similarly, map of the region *C* shows a broad (040) *r*YP peak, with maximum at $\Delta\omega\approx0.4°$, and a tail extending down to $\Delta\omega\approx-0.4°$. The (400) *r*YP reflection is also found, with a tilt $\Delta\omega\approx0.4°$. Less intense peaks attributed to *s*YP are also present.

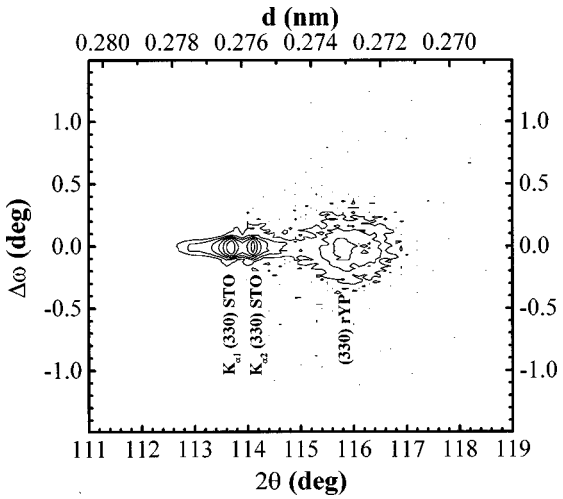

FIG. 7. Map of the region *A* after annealing of the sample performed following the procedure *a*.

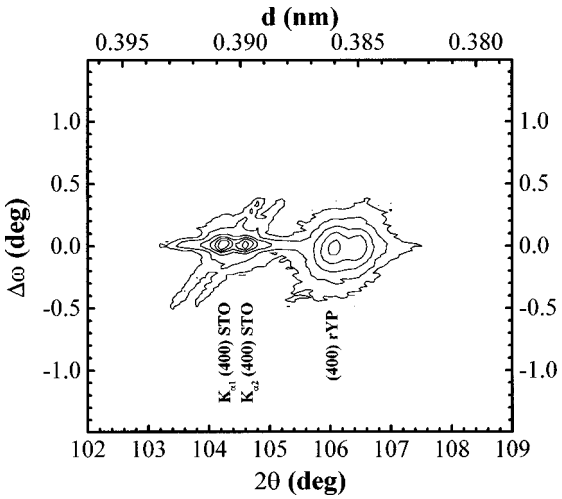

FIG. 8. Map of the region *B* after annealing of the sample performed following the procedure *a*. Due to the tetragonal symmetry YBCO/PBCO and STO axes are aligned.

IV. DISCUSSION OF THE EXPERIMENTAL RESULTS

Due to the rich variety of data emerging from our experiment and to the complexity of their interpretation, it is useful to itemize and discuss separately different aspects that will be addressed in the present section.

The presence of a strained (*s*YP) and of a relaxed (*r*YP) layer in the as-deposited film clearly emerges. The details of the epitaxial relations of the *a* and *b* axes of the two layers with respect to the substrate axes are addressed in Sec. IV A.

Comparison of asymmetric scan performed on regions *B* and *C* clearly shows that the film is essentially twin-free. Such a feature is correlated to the vicinal cut of the substrate in Sec. IV B.

A more complex situation emerges from the analysis of the sample annealed following procedures (a) and (b). Slight differences with respect to the as-deposited sample arise, implying that the rearrangement of axes orientation taking place during this second *T*-*O* transition does not reproduce exactly the behavior of the film during the cooling phase.

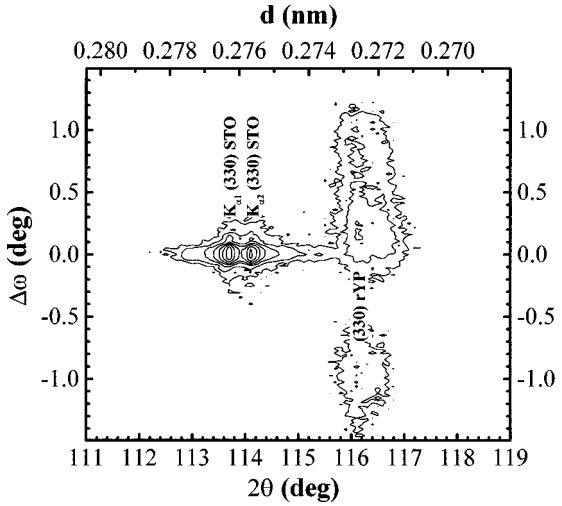

FIG. 9. Map of the region *A* after annealing of the sample, performed following the procedure *b*.

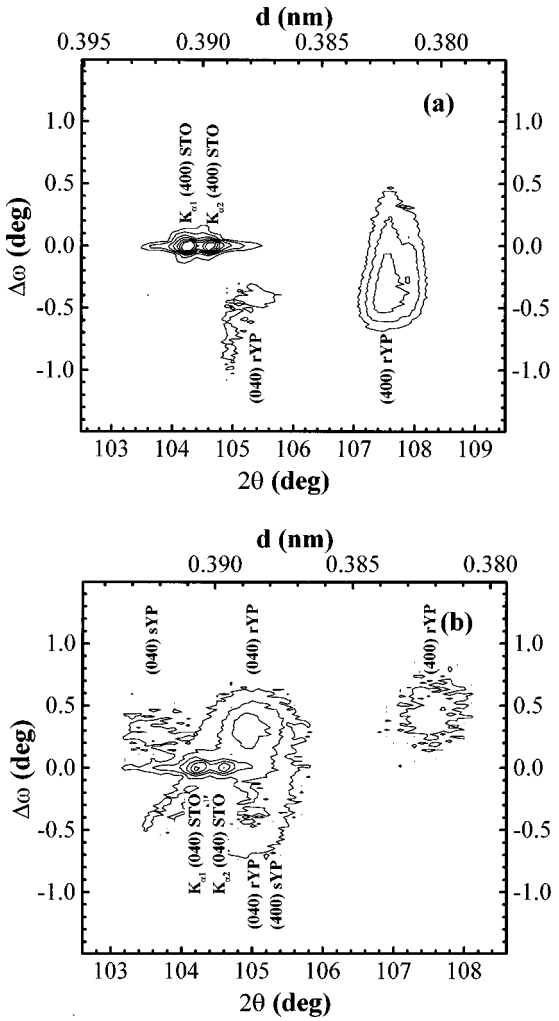

FIG. 10. Maps of regions *B* and *C* after annealing of the sample following the procedure *b*, are reported in (a) and (b), respectively.

Possible interpretations of this behavior will be reported in Sec. IV C.

A. Strained and relaxed layers

From the asymmetric scans reported in Figs. 6(a) and 6(b) the presence of two layers (*s*YP and *r*YP) possessing different lattice parameters has been deduced. As will be discussed in the following, the structure of the *s*YP layer is distorted in order to match the in-plane lattice of the (110) STO substrate. On the base of our data, it is not possible to state whether the interface between the *s*YP and the *r*YP layer corresponds to the YBCO/PBCO interface, or lies instead above it or behind it. It should be anyway noticed that the thickness of the PBCO film (50 nm) is well above the usual values of critical thickness for strain relaxation. For example, critical thickness of about 5 nm has been reported[19] for (001) YBCO on (100) STO. Some ambiguity in the interpretation arises from the uncertainty on the value of the relaxed PBCO *a*-and *b*- axes parameters. Contradictory values have been in fact reported on thin films[20] and powders.[21] The values reported in Ref. 21 are close within 0.2% to the YBCO *a* and *b* axes; the values reported in Ref. 20 are instead similar within experimental error to the *a* and *b* axes of our *s*YP

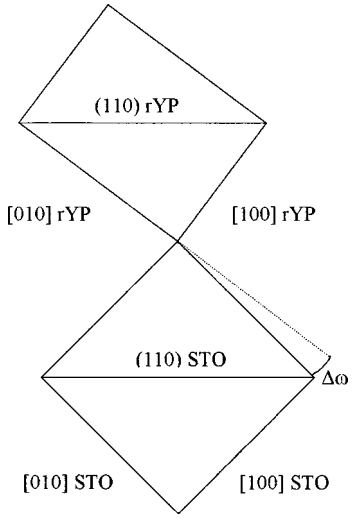

FIG. 11. Sketch reporting the orientation of the (110) cell of the *r*YP layer with respect to the (110) STO cell.

layer. Relying upon data from Ref. 20, we are inclined to believe that the *s*YP layer should be identified with the PBCO template, but such a hypothesis should be taken with due care.

Let us start analyzing the details of the epitaxial relation between the *r*YP layer and the substrate. By comparison with the sketches reported in Fig. 4, we can conclude that only one of the four epitaxial relations present on *c*-axis films is actually found in the case of (110) growth. The origin of the misalignment $\Delta\omega$ between the (100) *r*YP axis with respect to (100) STO, and of (010) *r*YP with respect to (010) STO, is explained in Fig. 11. The relation [110] *r*YP$\|$[110] STO is proved by the results of symmetrical map (Fig. 5). As a consequence, the *a*-*b* rectangle is tilted with respect to the square lattice of STO by $\Delta\omega = \arctan(b/a)$. This relation is satisfied by experimental results (see Table I).

In order to understand why only one of the four possible epitaxial relations illustrated in Fig. 4 is found, we observe that the symmetry for the exchange of the *a*-*b* axes is removed by the small tilt of the substrate plane with respect to the (110) plane. The role of such tilt in determining a preferential orientation of the *a* and *b* axes is discussed in the next section. Moreover, the symmetry between the [110] STO and the [110] STO directions is removed by the (110) cut. A simple explanation for the alignment of the (110) plane, rather than the (110) one, arises from the analysis of the sketch reported in Figs. 12(a)–12(c). It obvious that, during the *T*-*O* transition, the configuration having [110] *r*YP$\|$[110] STO is more easily obtained with respect to the one having [110] *r*YP$\|$[110] STO.

Let us turn now to the structure of the *s*YP layer. Define the angles θ_a and θ_b according to the relation $\theta_a = 45° + \Delta\omega_{(400)\ s\mathrm{YP}}$, $\theta_b = 45° + \Delta\omega_{(040)\ s\mathrm{YP}}$ (Fig. 13). The first interesting feature emerging from asymmetric maps [Figs. 6(a) and 6(b)] is that $\theta_a \neq \theta_b$ (Table I). Therefore, the *a* and *b* axes of the *s*YP cell are not perpendicular one to each other. A similar situation has already been observed on (001) YBCO films deposited onto (100) STO.[22] In order to study the details of the epitaxial relation between strained film and

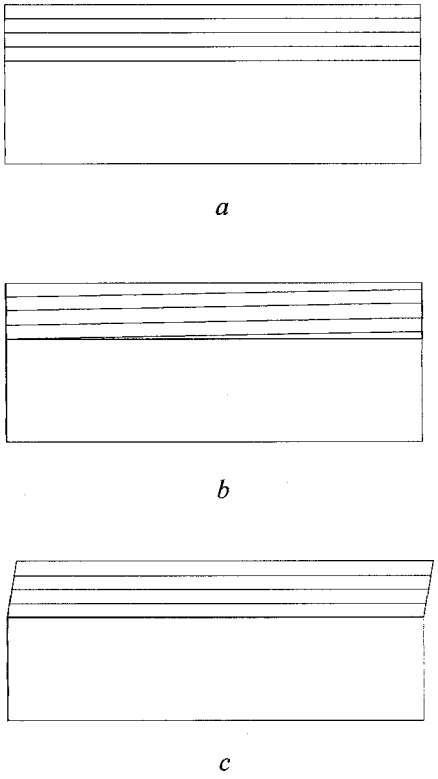

FIG. 12. Sketch reporting the deformation of the (110) YBCO planes during the *T*-*O* transition. The case of the tetragonal film is reported in (a). Two possible deformation taking place during the transitions are reported in (b) and (c). The condition $(1\bar{1}0)$ YBCO$\|$(110) STO is maintained in (b). The condition (110) YBCO$\|$(110) STO is instead maintained in (c). It is easily recognized that the transformation from structure (a) to structure (c) requires a less drastic atomic rearrangement.

substrate, we need to take into account the fact that the reciprocal lattice vector a^* is not parallel to the *a* axis anymore, due to the monoclinic distortion. The same holds for *b* and b^*. The distortion also causes a slight difference between the measured *d* spacing and the corresponding lattice parameter. Such effect is however below experimental sensitivity for both *a* and *b* axes.

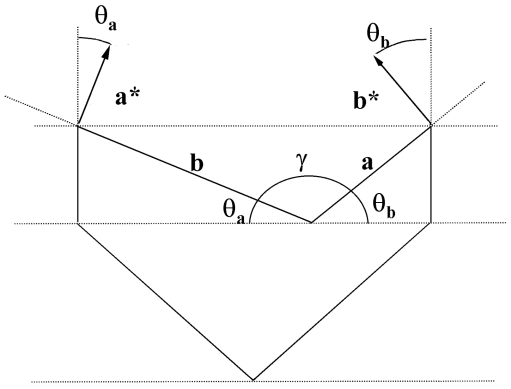

FIG. 13. Sketch reporting the epitaxial relation between the *s*YP layer (see text) and the STO substrate. The amplitude of the angle γ is 90.24°.

Two more results clearly emerge from a careful analysis of the experimental data. The following relations give strong support to our interpretation of the data, providing further internal consistence.

(i) In analogy with the case of the *r*YP layer, we expect the (110) planes of the *s*YP film to be parallel to the (110) planes of STO. As a consequence, it is deduced from geometrical considerations that

$$a\ \sin(\theta_b) = b\ \sin(\theta_a). \tag{1}$$

Data reported in Table I show that such relation is satisfied within 0.2%, which is comparable to experimental error.

(ii) In a fully strained layer, the relation

$$a\ \cos(\theta_b) + b\ \cos(\theta_a) = \sqrt{2} a_{\mathrm{STO}} \tag{2}$$

is expected to hold. Experimental data reported in Table I also fit such an equation within 0.07%, that is, within the uncertainty of our experimental values.

Equation (2) also allows an interpretation of the monoclinic distortion. In order to keep the orthorhombic structure, the lattice would have to stretch in such a way that the relation $a^2 + b^2 = 2a_{\mathrm{STO}}^2$ were satisfied. Moreover, a small rotation of the axes with respect to the principal directions of STO would be required in order to keep the relation (110) *s*YP$\|$(110) STO. The actual configuration is instead characterized by an angle γ that exceeds 90° ($\gamma = 90 + \Delta\omega_{(400)\ s\mathrm{YP}} + \Delta\omega_{(040)\ s\mathrm{YP}} = 90.24°$), and by a smaller spacing between (110) planes. It emerges, therefore, that the symmetry break due to monoclinization is permitted by the reduction of the elastic energy, due to the minor stretching of *a* and *b* axes.

As already stated, the film submitted to the thermal treatment *a* is tetragonal. The maps do not reveal the presence of distinct peaks that are attributed to strained YBCO/PBCO. Thus, it is possible to exclude the presence of a monoclinic structure. In fact, such a component would reveal itself by peaks shifted of some angle $\Delta\omega$ in the asymmetric maps. In conclusion, if a strained component is still present, it fits the STO layer almost perfectly.

B. The domain structure of *s*YP and *r*YP layers

It is well known that the steps on the substrate surface affect the growth mechanism of YBCO, as for instance in the case of (001) YBCO deposited on vicinal (100) STO.[23] Our experimental results indicate that the steps also influence the details of the *T*-*O* structural transition taking place during the cooling process. This statement is based on the comparison between the maps reported in Fig. 6(a) and 6(b). No (040) *r*YP reflections and very weak (040) *s*YP reflections are observed in the map of region *B*. As well, no (400) *r*YP reflections and very weak (400) *s*YP reflections are observed in the map of region *C*. From these measurements, we conclude that *a*-*b* axes twinning is suppressed in the *r*YP layer and strongly reduced in the *s*YP layer. Namely, the relative amounts of the *r*YP and *s*YP layers, with exchanged *a* and *b* axes, are below 1% and below 10%, respectively.

In the case of the (110) substrates considered in this work, the steps run parallel to the [001] STO direction. Previous analyses proved that the surface roughness of our crystals is quite low. Assuming that most steps have a height of 1 lattice spacing ($h \approx 2.76$ Å), an average distance between steps $D \approx 320$ Å is expected for a 0.5° miscut. The sketch reported in Fig. 14 shows the observed relation between axes orientation and steps on the substrate surface.

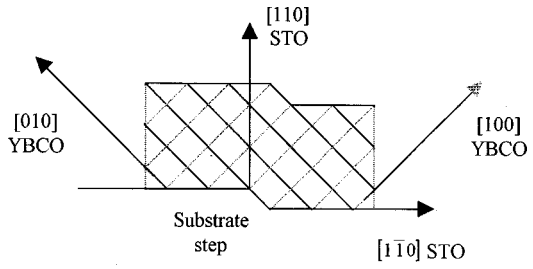

FIG. 14. Sketch reporting the growth of a twin-free (110) YBCO film on a vicinal (110) STO substrate. The presence of each step determines the formation of two extra (100) surfaces.

The oxygen ordering in the Cu-O planes of YBCO has been widely studied, both by experiment, and theory.[17,18] Detwinning of single crystals was achieved thermodynamically by applying uniaxial stresses of the order of 10^7 Pa at temperatures of the order of 300 °C, thus proving that YBCO is a ferroelastic material.[17] Also in the case of films, it is assumed that the twinning is essentially determined by thermodynamic properties. In fact, the diffusion of oxygen in the Cu-O planes is a fast process on the time scale of typical cooling procedures that are adopted to oxygenate the samples, so that the formation of the domains takes place close to equilibrium. The behavior of films is however more complex, because of the presence of the interface with the substrate. As already stated, experimental data prove that the twinning is influenced by the substrate type and by the growth orientation.

The effect of steps on the substrate surface can be described as follows. For simplicity, let us ignore the presence of a strained and a relaxed layer, which we believe to be irrelevant in a first-order approach. As well, we assume that YBCO and PBCO are equivalent from the point of view of surface energies. Looking at Fig. 14, it is recognized that the actual orientation of PBCO/YBCO axes is such, that the *b* axis runs parallel to the step edges. Therefore, due to the presence of a stepped surface, the absence of twin domains results in the formation of STO/PBCO interfaces and YBCO/vacuum interfaces all parallel to the (100) YBCO/PBCO planes. These *a*-axis interfaces related to the vicinal cut add to the other *a*- and *b*-axis interfaces, of equal area, due to roughness and faceting. We argue that the actual configuration is characterized by a lower surface energy, as it is discussed in the following.

The computation of interface energies requires a model of the boundary between the materials, as well as a microscopic description of the interaction between atoms. In order to get an estimate, we consider here a very simple model. The surface energy γ^{f-s} at the interface between film and substrate can be written in the form

$$\gamma^{f-s} = \gamma^f + \gamma^s - w^{f-s}, \tag{3}$$

where γ^f is the surface energy of the film; γ^s is the surface energy of the substrate; w^{f-s} is the reversible work necessary to divide the film from the substrate, including the con-

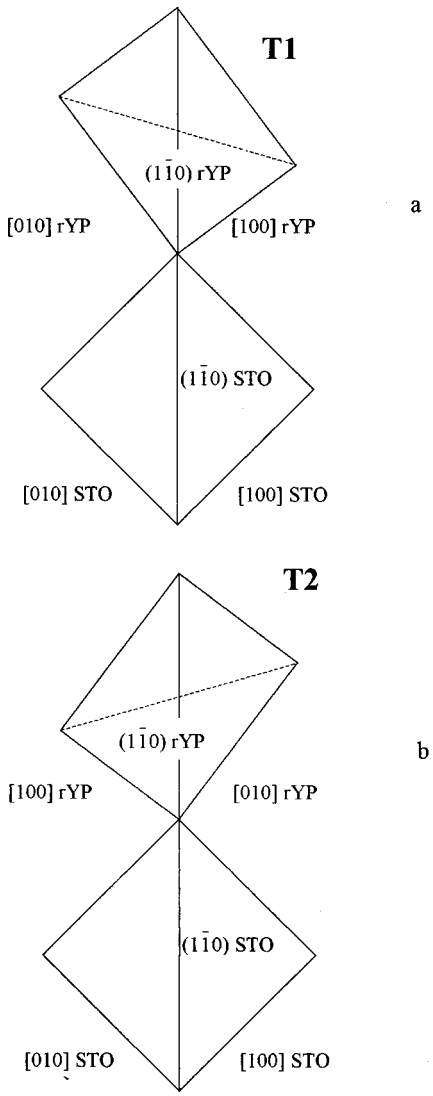

FIG. 15. Sketch reporting the epitaxial relation between the $T1$ and $T2$ orientations (see text) and the STO substrate.

tribution from relaxation. Assuming that w^{f-s} has the same value for both ''a-axis'' and ''b-axis'' interfaces, we get

$$\gamma_a^{f-s}-\gamma_b^{f-s}\approx\gamma_a^f-\gamma_b^f. \tag{4}$$

Also considering the contribution of the film-vacuum interfaces, which add an identical term, we can estimate the energy difference per unit volume between the configuration shown in Fig. 14 and the configuration in which a and b axes are exchanged, as

$$\Delta g=2(\gamma_a^f-\gamma_b^f)\,\frac{h}{Dt}, \tag{5}$$

where t is the film thickness.

Both theoretical and experimental evidence point to the conclusion that $\gamma_a^f<\gamma_b^f$.[24] Therefore, the creation of ''a-axis'' interfaces is more convenient in terms of surface energy. By considering (100) substrates as limiting cases of vicinal (110) substrates, the same mechanism explains why (100) orientation is usually preferred to (010) in c-axis in-plane YBCO films.[24,2] From theoretical estimations of Ref. 24, we get $\Delta g\approx10^4$ Jm^{-3}. Estimations of γ^f based on experimental data of single crystal indentation lead to $\Delta g\approx2.5\times10^4$ Jm^{-3} for a film with thickness $t=300$ nm.

The mechanism of detwinning can be interpreted as follows. In the state of minimum Gibbs energy, the sample does not show the presence of twinned domains, because they would be separated by walls that have some cost in term of surface energy. On the other hand, it is necessary to perform some irreversible work to remove the walls from a twinned sample. The generalized thermodynamic force that drives the system toward detwinning is Δg. It is interesting to compare this situation with the detwinning of single crystals under the action of an uniaxial stress p. In that case, the irreversible work per unit volume w made during the T-O transition is given by

$$w=p\epsilon, \tag{6}$$

where $\epsilon\approx1\%$ is the percent difference between a and b axes. For the typical value $p\approx10^7$ Pa,[17] we get $W\approx10^5$ Jm^{-3}, that is not very far from the estimates of Δg.

The same argument can be used to study the twinning of films with other orientation. For instance, single domain layers of (105) YBCO and PBCO are obtained by deposition onto (305) (STO).[25] This substrate may be considered as a ''vicinal'' (110) STO with about 19° tilt of [110] axis off [100] direction, so that the (105) YBCO and PBCO resemble (103) growth with similar tilt. Estimates of Δg are ≈40 times larger in this case. In the case of (100) STO with 4.5° tilt off [110] direction, we get $\Delta g\approx2-5\times10^5$ Jm^{-3} for a film with thickness $t=100$ mm. In spite of the larger driving force, such films are however twinned.[22] This circumstance confirms that the detwinning of c-axis films is more difficult, because of the large contributions of elastic energy.

C. Reversibility of the epitaxial relations during a deoxidation-oxidation cycle

The question of reversibility of the lattice rearrangement taking place during the T-O transition and described in the former sections has been addressed by analyzing the sample subjected to thermal cycling. The thermal treatment a described in Sec. A II brings the film to T symmetry. Thermal treatment b restores the O phase. During this latter process, ordering of a and b axes takes place. Comparison between Figs. 5 and 6 and Figs. 9 and 10 proves that the sample did not completely recover the same structure at the end of the whole process. The results are interpreted in the following: attention is only focused on the rYP layer.

A large fraction of the rYP film, to which we will refer in the following as the aligned fraction (AF), recovers the same epitaxial relation found in the as deposited film, that is, it shows [110] AF$\|$[110] STO and a single orientation of a and b axes. A minor fraction of the rYP layer is instead aligned with the [110] rYP direction tilted with respect to [110] STO, and will be referred to as tilted fraction (TF). The TF is composed of grains with different orientation: more precisely, part of the TF material seems to satisfy the epitaxial relation [110] TF$\|$[110] STO. Furthermore, the TF is twinned, thus leading to two possible configurations, indicated as $T1$ and $T2$ in the sketch reported in Figs. 15(a) and

15(b). Configurations corresponding to other tilt angles, which are somehow in between $T1$ and $T2$, are also present.

Let us show that the interpretation of the film structure in terms of AF and TF is fully confirmed by the maps reported in Figs. 9 and 10, and allows us to understand the different features that are obtained in the contour plots. We bring to mind that contour plots are in log scale, and that also reflection corresponding to a small fraction of the film may appear to be comparable to the principal peaks. As a matter of fact, the ratio between the TF and the AF of the material can be estimated on the basis of asymmetric maps to be $<10\%$:

(i) The presence of a dominant AF of the film is confirmed by the (330) rYP peak at $\Delta\omega\approx 0°$ in region A, the (400) rYP peak at $\Delta\omega\approx -0.4°$ in region B, and the (040) rYP peak $\Delta\omega\approx 0.4°$ in region C. The absence of the (400) rYP peak in region C, and of the (040) rYP peak in region B, proves that the AF of the film is twin- free.

(ii) The presence of a smaller twinned TF of the film is confirmed by the presence of a diffracted signal from the (330) peak in region A for $\Delta\omega$ in the interval $[-1.0°,1.0°]$, by the (040) at peak at $\Delta\omega\approx -0.4°$ in region B, the (400) peak at $\Delta\omega\approx 0.4°$ in region C and by the tails found on (400) and (040) AF peaks in regions B and C, respectively.

Our results suggest that the oxygen ordering in the a-b plane of (110) YBCO/PBCO is not strongly affected by differences in the cooling procedure. The origin of the minor TF ordering in the bilayer subjected to thermal treatments is not clear. However, notice that the thermal cycle b does not reproduce exactly the cooling process at the end of film deposition. Also due to the introduction of O_2 at very high temperatures soon after deposition, the T-O transition of as-deposited films takes place at a higher temperature, so that oxygen mobility is higher. Moreover, XRD analyses are not performed *in situ*, so that samples are subject to moisture between thermal cycles. The effects of contamination on YBCO are well known.[26] In our case, our sample is supposed to be extremely sensitive to contamination, since such effect is strongly enhanced both by oxygen deficiency (due to higher reactivity) and by c-axis in-plane orientation (due to the higher diffusion coefficients of chemical species along the a-b planes).

V. CONCLUSIONS

Structural and transport measurements confirm that high quality (110) YBCO films are obtained resorting to our double template technique. The samples are free of spurious phases or secondary orientations, such as (103)/(013), and show high values of the superconductive transition temperature.

Reciprocal space mapping performed by XRD has been employed to investigate the details of the bilayer structure. The main results that have been achieved regard the understanding of the mechanism of strain relaxation and of the origin of detwinning. Our measurements clearly point to the conclusion that (110) YBCO/PBCO bilayers are characterized by the presence of a strained layer, above which a fully relaxed film is grown. The strained part presents a monoclinic distortion of the structure. This feature allows YBCO/PBCO to fit the STO lattice, in such a way that the [110] directions coincide, and the in-plane lattices are exactly overlapped. The relaxed component is also characterized by the relation $[110]\,\mathrm{YBCO/PBCO}\|[110]\,\mathrm{STO}$. The rectangular a-b sublattice is arranged in such a way that the a and b axes form an angle $\Delta\omega=0.45°$ with homologous axes of STO.

We also investigated the details of the oxygen ordering in the Cu-O planes of the YBCO/PBCO film grown on vicinal (110) STO. Our experimental evidence proves that the domain structure of the samples is influenced by the presence of steps on the substrate. In particular, a single domain YBCO/PBCO film was obtained by deposition onto a substrate presenting a 0.5° tilt of the [110] axis off [100] direction. We argue that detwinning of the films takes place under the effect of a driving force that exerts a uniaxial pressure. This force is determined in our case by the presence of the steps that break the symmetry of the substrate plane. As a consequence, the alignment of the YBCO/PBCO a axis along one direction is energetically favored. This process is not inhibited by strain effects in (110) films, in contrast with the case of (001) films.

The oxygen ordering is a reversible process. Our results prove that the largest part of a bilayer recovers the same domain structure after a thermal cycle involving O-T and T-O transitions. However, the displacement of the walls that separate domains with different twinning is not reversible, so that some details of the structure can be influenced by dynamical effects. In particular, oxygen ordering of as-deposited films takes place during the cooling process. Our thermal cycle involved a lower annealing temperature, and therefore a lower oxygen mobility in the Cu-O planes, with respect to the cooling process performed soon after deposition. This circumstance may explain some differences between the structure of as-made and of treated samples. However, some caution is required in the interpretation of experimental data, as the influence of moisture contamination cannot be ruled out.

ACKNOWLEDGMENTS

This work has been partially supported by European Community through the Human Capital Mobility Network on Physics of Three Terminal High-T_c Devices and the ESPRIT-BR ''HTS-WELITTD'' Project. We gratefully acknowledge Dr. I. Schuster for scientific discussions.

*Author to whom correspondence should be addressed. Electronic address: miletto@na.infn.it

[1] J. Geerk, G. Linker, O. Meyer, F. Ratzel, J. Reiner, J. Remmel, T. Kroner, R. Henn, S. Massing, E. Brecht, B. Strehlau, R. Smithey, R. L. Wang, F. Wang, M. Siegel, C. Ritschel, and B. Raushenbach, Physica C **180**, 11 (1991); A. Inam, R. Ramesh, C. T. Rogers, B. Wilkens, K. Remshnig, D. Hart, and J. Barner, IEEE Trans. Magn. **27**, 1603 (1991).

[2] A. Cassinese, A. Di Chiara, F. Miletto Granozio, S. Saiello, U. Scotti di Uccio, and M. Valentino, J. Mater. Res. **10**, 11 (1995).

[3] S. Poelders, R. Auer, G. Linker, R. Smithey, and R. Schneider, Physica C **247**, 309 (1995).

[4] J. P. Krumme, V. Doorman, F. Welz, R. Eckart, O. Dössel, W. Dingen, and K. Shiffmann, J. Mater. Res. **9**, 3032 (1994).
[5] S. Hontsu, J. Ishii, T. Kawai, and S. Kawai, Appl. Phys. Lett. **59**, 2886 (1991); Y. Suzuki, D. Lew, A. F. Marshall, M. R. Beasley, and T. H. Geballe, Phys. Rev. B **48**, 10 642 (1993); Masashi Mukaida and Shintaro Miyazawa, Appl. Phys. Lett. **63**, 999 (1993).
[6] J. Z. Wu, P. Y. Hsieh, A. V. McGuire, D. L. Schmid, L. T. Wood, Y. Shen, and W. K. Chu, Phys. Rev. B **44**, 12 643 (1991).
[7] M. Covington, R. Scheuerer, K. Bloom, and L. H. Greene, Appl. Phys. Lett. **68**, 1717 (1996).
[8] J. W. Seo, B. Kabius, C. L. Jia, H. Soltner, U. Poppe, and K. Urban, Physica C **225**, 158 (1994).
[9] H. U. Habermeier, A. A. C. S. Lourenço, B. Friedl, J. Kircher, and J. Köhler, Solid State Commun. **77**, 683 (1991).
[10] C. B. Eom, A. F. Marshall, Y. Suzuki, T. H. Geballe, B. Boyer, R. F. Pease, R. B. van Dover, and J. M. Philips, Phys. Rev. B **46**, 11 902 (1992).
[11] A. Inam, C. T. Rogers, R. Ramesh, K. Remschnig, L. Farrow, D. Hart, T. Venkatesan, and B. Wilkens, Appl. Phys. Lett. **57**, 2484 (1990).
[12] C. B. Eom, A. F. Marshall, S. S. Laderman, R. D. Jacowitz, and T. H. Geballe, Science **249**, 1549 (1990).
[13] E. Olsson, A. Gupta, M. D. Thouless, A. Segmüller, and D. R. Clarke, Appl. Phys. Lett. **58**, 1682 (1991); C. Rossel, A. Catana, R. R. Schulz, E. J. Williams, A. Perrin, M. Guilloux-Viry, and C. Thivet, Physica C **223**, 370 (1994).
[14] J. D. Budai, R. Feenstra, and L. A. Boatner, Phys. Rev. B **39**, 12 355 (1989).
[15] J. Sapriel, Phys. Rev. B **12**, 5128 (1975); Hoydoo You, J. D. Axe, X. B. Kan, S. C. Moss, J. Z. Liu, and D. J. Lam, *ibid.* **37**, 2301 (1988).
[16] T. Scherer, P. Marienhoff, R. Hervig, M. Neuhaus, and W. Jutzi, Physica C **197**, 79 (1992).
[17] D. Favrot, M. Déchamps, and A. Revcolevschi, Philos. Mag. Lett. **64**, 147 (1991); H. Schmidt, E. Burkhardt, B. N. Sun, and J. P. Rivera, Physica C **157**, 555 (1989); D. L. Kaiser, F. W. Gayle, R. S. Roth, and L. J. Swartzendruber, J. Mater. Res. **4**, 745 (1989).
[18] C. P. Burmester, L. T. Wille, and R. Gronsky, Physica C **230**, 16 (1994), and references therein; A. A. Aligia, H. Bonadeo, and J. Garces, Phys. Rev. B **43**, 542 (1991); G. W. Morris, E. J. Tomlinson, R. E. Somekh, Z. H. Barber, E. J. Williams, M. P. Ray, and J. E. Evetts, IEEE Trans. Magn. **27**, 1430 (1991).
[19] D. Huettner, O. Meyer, J. Reiner, and J. Linker, Appl. Phys. Lett. **66**, 1273 (1995).
[20] I. Takeuchi, Z. Trajanovic, J. L. Peng, Z. Y. Li, S. N. Mao, P. A. Warburton, C. J. Lobb, and T. Venkatesan, IEEE Trans. Appl. Supercond. **5**, 2365 (1995); M. E. Lòpez-Morales, D. Rìos-Jara, L. Tagüeña, R. Escudero, S. La Placa, A. Bezinge, V. Y. Lee, E. M. Engler, and P. M. Grant, Phys. Rev. B **41**, 6655 (1990).
[21] Powder Diffraction File (JCPDS International Center for Diffraction Data, Swarthmore, PA) Pattern no. 45-216.
[22] V. P. Martovitsky and V. V. Rodin, Physica C **182**, 269 (1991).
[23] S. J. Pennycook, M. F. Chisolm, D. E. Jesson, R. Feenstra, S. Zhu, X. Y. Zheng, and D. J. Lownes, Physica C **202**, 1 (1992).
[24] F. Miletto Granozio and U. Scotti di Uccio, J. Alloys Compd. **251**, 332 (1997).
[25] W. A. M. Aarnink, E. M. C. M. Reuvekamp, M. A. J. Verhoeven, M. V. Pedyash, G. J. Gerritsma, A. van Silfhout, H. Rogalla, and T. W. Ryan, Appl. Phys. Lett. **61**, 607 (1992).
[26] A. Andreone, A. Di Chiara, U. Scotti di Uccio, F. Miletto Granozio, M. Valentino, G. Condorelli, G. Malandrino, and I. Fragala, in *Superconductors and Superconducting Materials Technologies*, edited by P. Vincenzini (Techna s.r.l., Florence, Italy, 1995), p. 165.